Control of propagating spin-wave attenuation by the spin-Hall effect

Citation: Woo, Seonghoon and Geoffrey S. D. Beach. "Control of Propagating Spin-Wave Attenuation by the Spin-Hall Effect." Journal of Applied Physics 122, 9 (September 2017): 093901

As Published: http://dx.doi.org/10.1063/1.4999828

Publisher: American Institute of Physics (AIP)

Persistent URL: http://hdl.handle.net/1721.1/118407

Version: Final published version: final published article, as it appeared in a journal, conference proceedings, or other formally published context

Control of propagating spin-wave attenuation by the spin-Hall effect

Seonghoon Woo, and Geoffrey S. D. Beach

Citation: Journal of Applied Physics **122**, 093901 (2017); doi: 10.1063/1.4999828
View online: http://dx.doi.org/10.1063/1.4999828
View Table of Contents: http://aip.scitation.org/toc/jap/122/9
Published by the American Institute of Physics

Control of propagating spin-wave attenuation by the spin-Hall effect

Seonghoon Woo[a),b)] and Geoffrey S. D. Beach
Department of Materials Science and Engineering, Massachusetts Institute of Technology, Cambridge, Massachusetts 02139, USA

(Received 15 March 2017; accepted 10 August 2017; published online 1 September 2017)

The spin-Hall effect induced modification of the attenuation of propagating exchange-mode spin waves (SWs) is studied micromagnetically and analytically in heavy-metal/ferromagnet bilayers. Micromagnetic simulations of spin-wave propagation in Pt/NiFe show that at a relatively low current density of $\sim 6 \times 10^{11}$ A/m^2, Gilbert damping is exactly balanced by the spin-Hall torque and long-distance SW transmission is possible. An analytical model is developed to explain the micromagnetic results and relate the current density to the characteristic attenuation length. The results suggest that the spin Hall effect can be used as an effective means to control the attenuation length of propagating spin waves in nanostructures. *Published by AIP Publishing.*
[http://dx.doi.org/10.1063/1.4999828]

I. INTRODUCTION

Spin waves (SWs) are the collective spin excitations in a magnetic material. They are of great fundamental and technological interest due to their central role in magnetization dynamics and the possibility to exploit them for signal transmission and processing in spintronic devices.[1–13] Low-damping alloys[1–3] and garnet films[4–6] have provided model systems for examining SW phenomena and devices due to the large SW attenuation length in these materials. However, many recent modeling efforts have focused instead on metallic ferromagnets, in which the very short wavelength of dipole-exchange mode spin waves (DESWs) makes them better-suited for nanoscale magnonic devices.[7–9] It has been shown through micromagnetic simulations that nanostructured metallic ferromagnets can be engineered to act as spin-waveguides and magnonic crystals for signal interconnects,[10] filtering,[11] and logic.[12,13] Moreover, SWs can interact with magnetic domain walls,[14–17] allowing for hybrid spintronic architectures combining information storage and transmission capabilities.[17] Unfortunately, realizing such devices experimentally is challenging due to the relatively large damping in transition metal ferromagnets, which limits the attenuation length to typically a few micrometers or less.

Recent micromagnetic studies have demonstrated SW amplification using non-adiabatic spin-transfer torque (STT) generated by spin-polarized current flowing through a metallic ferromagnet.[18] Current-induced SW amplification could be used to counter intrinsic damping and enhance the propagation distance of SWs in devices, while also adding new functionality. However, significant amplification was only predicted at extremely high current densities with a large nonadiabicity parameter,[18] which may be difficult to achieve experimentally. More recently, the spin torque from the spin Hall effect (SHE) in nonmagnetic heavy metals (HMs) such as Pt,[19–21] Ta,[21,22] and W[23] has been shown capable of exciting magnetization dynamics and large-amplitude switching in an adjacent ultrathin FM when a relatively low current density flows parallel to the interface. This effect produces a Slonczewski-like antidamping torque[24,25] that can counteract damping and drive the magnetization away from equilibrium. Using optical and electrical measurement techniques, several early experiments have proved that the Slonczewski-like torque induced by the SHE could indeed modulate the amplitude of propagating dipole SWs in HM/ferromagnet bilayers such as Pt/CoFeB,[26] Ta/CoFeB,[27] Pt/YIG,[28] and Pt/Py.[29]

In this work, we first show through micromagnetic simulation that the SHE is sufficient to provide a practical means to achieve current-controlled amplification/attenuation of DESWs as was studied experimentally in Refs. 26–29. Moreover, we reveal that the SHE-driven torque can exactly balance the Gilbert damping at a certain critical current density, leading to extremely long-range propagation of SWs. Finally, using an analytical approach, we develop a simple equation for the effective SW attenuation length in such HM/ferromagnet bilayers under the influence of the SHE, which can be used to engineer the properties of propagating SWs in magnonic devices.

II. SIMULATION METHODS

A Pt/$Ni_{80}Fe_{20}$ bilayer, similar to that experimentally studied in Ref. 29, was chosen as a typical heavy-metal/ferromagnet bilayer for these studies. We considered a nanostrip geometry, shown schematically in Fig. 1(a), in which a charge current flowing parallel to the interface generates a vertical spin current with incident spin polarization along the $\hat{y}$-axis. The ratio of vertical spin-current to in-plane charge current is given by the spin Hall angle, θ_{SH}. This spin current exerts a Slonczewski-like torque $\vec{\gamma}_{SLT}^{SHE}$ on the ferromagnet of the form

$$\vec{\gamma}_{SLT}^{SHE} = \gamma \vec{m} \times \left[\frac{\hbar \theta_{SH} j_a}{2\mu_0 e M_S L_z} \vec{m} \times \hat{y} \right]. \quad (1)$$

[a)]Present address: Center for Spintronics, Korea Institute of Science and Technology, Seoul 02720, South Korea
[b)]Author to whom correspondence should be addressed: shwoo_@kist.re.kr

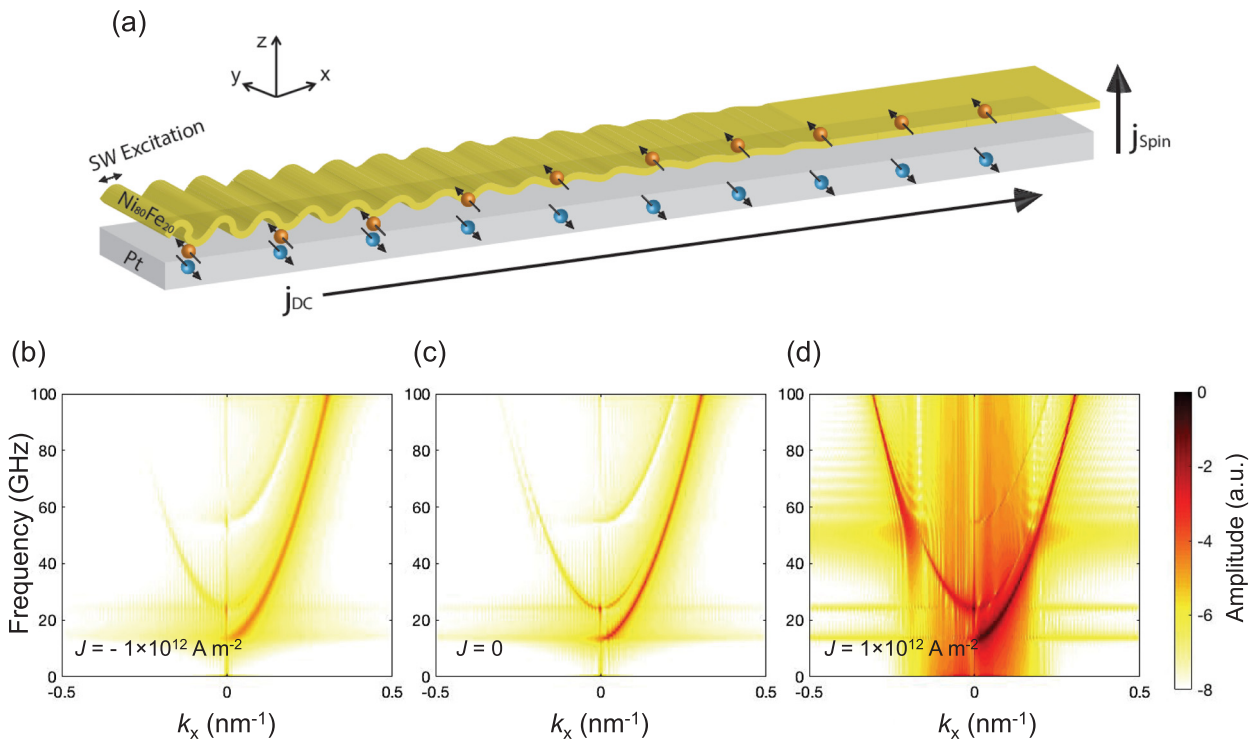

FIG. 1. (a) Schematic of $Pt/Ni_{80}Fe_{20}$ nanowire used for simulations, showing the area used for SW excitation and pure spin-injection driven by spin-Hall effect (SHE). Fast Fourier transform (FFT) power spectrum of the z-component of the magnetization in a wire at (b) $j_{DC} = -1 \times 10^{12}$, (c) $j_{DC} = 0$, and (d) $j_{DC} = +1 \times 10^{12}$ A/m^2, respectively.

Here, j_a is the charge current density, M_s is the ferromagnet saturation magnetization, L_z is the ferromagnet thickness, e is the electron charge, γ is the gyromagnetic ratio, μ_0 is the vacuum permeability, $\hbar$ is the reduced Planck constant, and $\vec{m} = \vec{M}/M_s$ is the normalized magnetization. We used a spin-Hall angle $\theta_{SH} = +0.07$, corresponding to the value for Pt reported in Ref. 19.

Magnetization dynamics was examined by incorporating this torque into the Landau-Lifshitz-Gilbert (LLG) equation[30,31]

$$\frac{\partial \vec{m}}{\partial t} = \gamma \vec{m} \times \vec{H}_{eff} + \alpha \vec{m} \times \frac{\partial \vec{m}}{\partial t} + \vec{\gamma}_{SLT}^{SHE}, \qquad (2)$$

where α is the Gilbert damping constant and $\vec{H}_{eff}$ is the net effective field, including applied, exchange, anisotropy, and dipolar fields.

We first examine the effect of current injection on SW propagation through micromagnetic simulations. Simulations were performed for a 2 μm long, 30 nm wide, 1 nm thick $Ni_{80}Fe_{20}$ strip, using the Object Oriented Micromagnetics Framework (OOMMF)[32] with the cell size of $2.5 \times 2.5 \times 1$ nm^3. The materials parameters were chosen to be those of Permalloy ($\alpha = 0.01$, exchange constant $A = 1.3 \times 10^{-11}$ J/m, and $M_s = 8 \times 10^5$ A/m). Vertical spin current injection by the SHE was implemented in OOMMF by using a second ferromagnetic spin polarizing layer magnetized along +x, with vertical current flow, and with current densities scaled so that the spin current corresponds to what would be generated by the current densities reported here when flowing in a Pt layer with the specified spin Hall angle. Note that the damping constant of 0.01 used for convenience in this simulation, which is known as the typical damping constant of Py thin films, might be too small for such an ultrathin Py layer placed in contact with Pt, due to spin pumping enhancement of the damping. However, it is possible experimentally to insert spin-transparent layers between Pt and the ferromagnet to reduce this effect[5,33,34] or use a different spin Hall metal such as Ta, which has been found not to increase the effective damping of the ferromagnet it is in contact with.[22] Moreover, the exact value of the damping constant only influences the results quantitatively without affecting on the main idea emphasized throughout this study.[35] Due to the form of the Slonczewski-like torque, the transverse spin polarization of the SHE-generated spin current will tend to amplify or damp local precessional motion about $\hat{y}$ due to SW excitations. We therefore imposed an in-plane transverse anisotropy (which is localized to the Py layer) so that the magnetization orients along $\hat{y}$ in equilibrium and thus injected current can maximally amplify or attenuate SWs. A relatively large anisotropy field H_k=10 kOe was used to ensure saturation along the transverse direction for convenience, but in practice, a static transverse bias field could be used to ensure a significant component of the magnetization along $\hat{y}$.

III. RESULTS AND DISCUSSION

SW amplification was studied by using a SW source consisting of a row of cells at the left-end of the nanowire excited by a time-varying field $H_x = H_0 \frac{\sin(2\pi\nu t)}{2\pi\nu t}$, where H_0=10 kOe and ν = 100 GHz. Such a large field amplitude of H_0=10 kOe was chosen to effectively perturb the

magnetization of Py, since a strong anisotropy field of H_k=10 kOe was used. This sine cardinal function serves to equally excite all modes of SWs up to ν, so that the spectral dependence of current-induced effects can be examined. While this excitation was applied, a dc-current through the Pt layer was simulated by injecting a spin current vertically proportional to θ_{SH} (as described above). Figures 1(b)–1(d) show the Fast Fourier transform (FFT) of the z-component (out of plane) magnetization within the entire area of nanowire computed for a time interval of 2 ns after the external Oersted field was applied. Excitation spectra are shown for dc-currents corresponding to $j_{DC} = -1 \times 10^{12}$ A/m^2, $j_{DC} = 0$, and $j_{DC} = +1 \times 10^{12}$ A/m^2, respectively. The parabolic relation between the frequency (f) and the wave vector (k) is observed in all cases, corresponding to the dispersion relation of dipole-exchange mode SWs. A lower cutoff frequency near $f \sim 15$ GHz, which appears due to the lowest transverse standing wave mode k_y in a confined geometry,[9] is also observed. Note that our geometrical configuration falls in the Damon-Eshbach[36] geometry where the SW wave vector is perpendicular to the magnetization of Py. However, the Damon-Eshbach SWs, which are dominated by dipolar interactions that exhibit a linear dispersion relation for small wave numbers and disappear as the exchange-dominated SWs from the Heisenberg interaction emerge at larger wave numbers,[37,38] are not observed in our SW spectrum. The inhibition of dipole-dominated SWs in our case is due to the small thickness of the simulated Py, t_{Py}=1 nm, which suppresses the portion of initial linear dispersion dominated by bulk contribution. Thus, SWs in this study appear with a quadratic dispersion relation and thus can be regarded as only exchange-dominated SWs. With no injected current [Fig. 1(c)], SWs propagating along the +x direction were dominantly observed as the spectrum is obtained to the right of the SW source. Note that the value of k_y is quantized due to the confined width of the nanowire, $w \sim 30$ nm, while the value of k_x is rather continuous, yielding the total wave number $\boldsymbol{k}^2 = {k_x}^2 + {k_{y,m}}^2$ with m = 1, 2, etc. Thus, the lowest quadratic branch right above $f \sim 14$ GHz corresponds to SWs traveling primarily along the x-axis, where the quantized k_y has its smallest value, $k_{y,m}$ with m = 1. There also exist other quadratic branches with much reduced contrast at higher frequencies, corresponding to the forward and backward SWs with $k_{y,m}$ having m = 2, 3, etc.[9] The backward SW modes, k_x<0, appeared because some portion of SWs reached the end of the nanowire and reflected. At $j_{DC} = +1 \times 10^{12}$ A/m^2 [Fig. 1(d)], the amplitude of FFT power is significantly enhanced and much stronger k_x<0 modes are observed, implying the largely reduced SW attenuation along the wire. It is also observed that the largest amplitude of backward SWs is observed for $k_{y,m}$ with m = 2. By contrast, with $j_{DC} = -1 \times 10^{12}$ A/m^2 [Fig 1(b)], faint k_x>0 modes are only observed, with a reduced amplitude as compared to the zero-current case. These data indicate that current acts to amplify or attenuate the propagating SWs, depending on the current direction and hence the sign of the anti-damping Slonczewski-like torque in Eq. (1).

In order to examine the influence of the SHE on the SW attenuation length in more detail, we examined the position-dependent SW amplitude for a discrete excitation frequency, under varying current densities. Here, we excited the SW mode at frequency $\nu = 50$ GHz, by applying $H_x = H_0 \sin(2\pi\nu t)$, with H_0=1 kOe. Unlike the previous simulation set, the field frequency has been changed to $\nu = 50$ GHz, which is safely below the upper frequency examined above and closer to an experimentally accessible value. The field was applied to the same row of cells as the case of sine cardinal function and the area and time of simulation were also identical. Figures 2(a)–2(d) shows the SW spectral intensity versus the distance from SW source, computed from FFT of rows of cells at varying position along the nanowire, at $j_{DC} = -3 \times 10^{11}$, $j_{DC} = 0$, $j_{DC} = +3 \times 10^{11}$, and $j_{DC} = +6 \times 10^{11}$ A/m^2, respectively. From these figures, for $j_{DC} < 6 \times 10^{11}$ A/m^2, it is evident that current has no significant effect on the SW frequency, but markedly changes the attenuation length. However, at $j_{DC} = 6 \times 10^{11}$ A/m^2, it is observed that SWs propagate to the end of nanowire without noticeable attenuation, and additional strong SWs appear at lower frequencies, $f < 50$ GHz. The low-f SWs may arise near nanowire edges because the restricted geometry induces strongly localized low-f SW modes in the excitation spectrum as studied in Refs. 39 and 40. This is reasonable because SWs can propagate to the end of nanowire edges while maintaining large amplitude at $j_{DC} = 6 \times 10^{11}$ A/m^2, implying sizable SW-edge interactions. Figure 2(e) shows the SW amplitude versus distance at various current densities. It is clear that current injection along the nanowire significantly enhances or reduces the SW attenuation length depending on the current polarity, consistent with a current-induced (anti)damping-like torque. With no applied current, the intensity of SWs is reduced exponentially by a factor of $\sim$100 at $d = 2\,\mu$m. However, with $j_{DC} = +6 \times 10^{11}$ A/m^2, the SHE-driven effective torque exactly balances the Gilbert damping and the SW intensity is maintained at the same level along the 2 μm length. This negligible SW attenuation is also in good agreement with the simulation result presented in Fig. 2(d). At $j_{DC} > +6 \times 10^{11}$ A/m^2, the SW attenuation becomes negative, and therefore the SW amplitude exponentially grows and the uniformly-magnetized state is destabilized further along the nanowire, causing chaotic magnetization dynamics as described in more detail below.

In order to provide further insight into spin-Hall torque-induced spin-wave attenuation, here we provide a simple analytical relation. From a similar approach used in Ref. 18, where the nonadiabacity of the spin transfer torque was considered as an additional torque term within the LLG equation, we can draw a simple relation for our case, where the spin Hall torque is considered instead of a nonadiabatic torque. With the assumption of small damping, the SHE-induced modulation of spin wave attenuation length becomes

$$\lambda \propto \frac{1}{\alpha w_f - \Pi j_a}, \tag{3}$$

where λ is the characteristic attenuation length, ω_f is the angular frequency, and Π is the constant coefficient of a Slonczewski-like torque as shown in Eq. (1), where

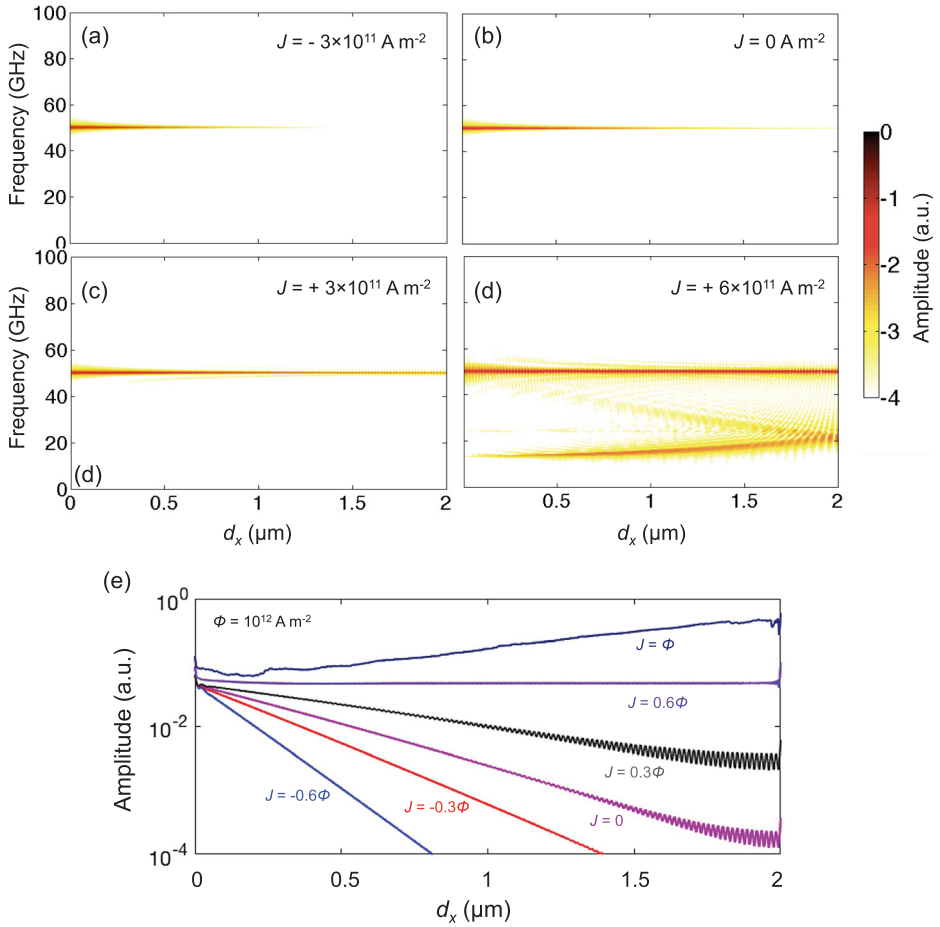

FIG. 2. Fast Fourier transform (FFT) power spectrum of the z-component of the magnetization in a wire depending on the position at **(a)** $j_{DC} = -3 \times 10^{11}$, **(b)** $j_{DC} = 0$, **(c)** $j_{DC} = +3 \times 10^{11}$, and **(d)** $j_{DC} = +6 \times 10^{11}$ A/m^2, respectively. **(e)** SW amplitude change with a distance in a wire calculated at various in-plane current densities, where j_{DC} varies from $j_{DC} = -3 \times 10^{12}$ to $j_{DC} = +1 \times 10^{11}$ A/m^2.

$\Pi = \frac{\hbar\gamma\theta_{SH}}{2\mu_0 M_S L_z}$. Because the term $\alpha\omega_f$ implies the SW relaxation rate in the presence of damping, Eq. (3) represents the spin-Hall current-induced change of the SW attenuation length, which is reasonably expected and also analytically studied in Ref. 29. Because the term Π is directly proportional to the spin Hall angle, θ_{SH}, it is evident that the SHE can compensate the intrinsic damping and thus can modulate the SW attenuation. Moreover, the attenuation length diverges when $\alpha w_f = \Pi j_a$, and this state can be achieved by increasing the current density at a given frequency of SWs and the spin Hall angle. In Fig. 2(d), we have observed that SHE can exactly compensate the Gilbert damping near $j_{DC} = +6 \times 10^{11}$ A/m^2 and the critical current density using the derived equation, where $\alpha w_f = \Pi j_a$, is $j_c = +6.2 \times 10^{11}$ A/m^2, which agrees with the simulation result.

In Fig. 2(d), we extract the attenuation length from the micromagnetically computed SW amplitude versus position as $\frac{\partial \ln A_{SW}}{\partial d} = -\frac{1}{\lambda}$, where A_{SW} is the amplitude of propagating SWs. In Fig. 3, we plot these data versus current density, as well as the analytical result for $-1/\lambda$ using Eq. (3). Figure 3 shows good agreement between the full micromagnetic calculations and the analytical result, indicating that Eq. (3) captures the essential physics responsible for SHE-induced SW attenuation.

With $j_{DC} > j_c$, a negative attenuation length can be estimated from Eq. (3), corresponding to amplification of the SW amplitude with increasing distance from the SW source as seen in Fig. 2(d). In this case, chaotic magnetization dynamics ensues distant from the SW source, and with increasing time, the transition to chaotic dynamics moves progressively towards the SW source. Figures 4(a) and 4(b) show micromagnetic snapshots with increasing time after applying Oersted field to excite SWs to the left, in the case of zero current density and $j_{DC} > j_c$, respectively. It is evident that the negative attenuation predicted for $j_{DC} = +1 \times 10^{12}$ A/m^2 above a threshold indeed drives a transition to chaotic dynamics. In detail, the superposition between the propagating SWs from the source and reflected SWs from the right edge of the nanowire leads to local standing waves

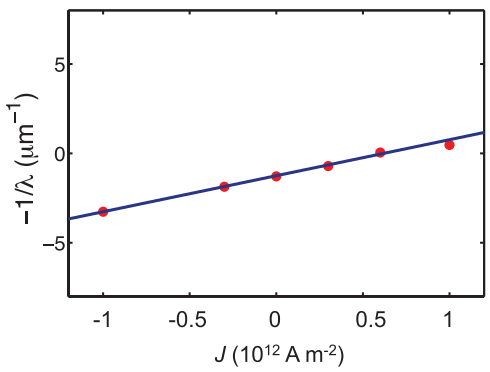

FIG. 3. The characteristic SW attenuation length versus charge current density calculated by micromagnetic simulation (red dots) and an analytical equation (blue line).

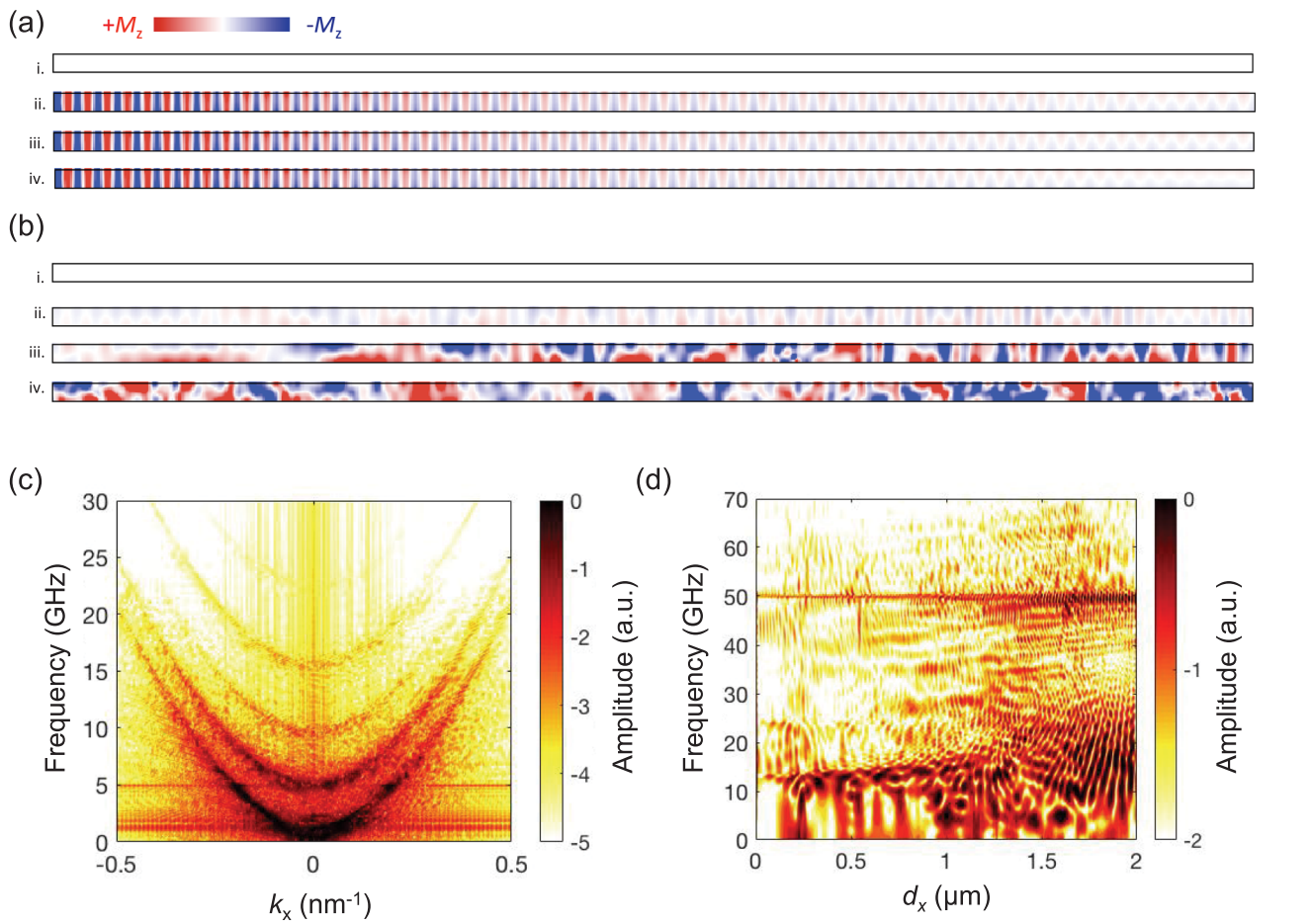

FIG. 4. Magnetization textures after applying Oersted field to excite SWs to a row of cells at the left-end of the nanowire. **(a)** i-iv correspond to the case of zero current density at **i.** t = 0 ns, **ii.** 1 ns, **iii.** 1.5 ns, and **iv.** 2 ns, respectively. **(b)** i-iv are snapshots in the case where $j_{DC} = +1 \times 10^{12}$ A/m^2 at **i.** t = 0 ns, **ii.** 1 ns, **iii.** 1.5 ns, and **iv.** 2 ns, respectively. Fast Fourier transform (FFT) power spectrum of the z-component of the magnetization as a function of **(c)** wave number and **(d)** the distance from the left-end wire edge, respectively.

within the nanowire structure. As time evolves, the amplitude of the local standing SWs becomes much stronger, and eventually overtakes the entire structure, eventually turning into random domain nucleation and expansion. Figures 4(c) and 4(d) show the Fast Fourier transform (FFT) of the z-component (out of plane) magnetization as a function of wave number and wire position, respectively. It is first obvious that strong local low-frequency SW modes, which should be forbidden due to the geometrical confinement, are observed for the chaotic dynamics. The low-frequency modes, which were also shown in Fig. 2(d), correspond to the local SWs arising from the edges, and Fig. 4(d) indeed exhibits the evolution of strong low-frequency modes from the wire edge, where the interaction between forward and backward SWs is the strongest. This behavior suggests that SWs may likewise play an important role in SHE-induced switching, since they tend to destabilize the uniform state and can be amplified by the switching current.

IV. CONCLUSION

In conclusion, micromagnetic simulations predict DESW amplification and attenuation driven by the SHE torques at relatively low current density using spin Hall angles that are readily achieved with known spin Hall metals. Analytical modeling gives a simple expression for the SW attenuation length dependence on current density and spin Hall angle, which reproduces well the full micromagnetic results. These results show that the spin Hall torque can be harnessed for SW amplification, allowing for a means to overcome damping for long-distance SW signal transmission and providing an electrical means to control SW devices.

ACKNOWLEDGMENTS

This work was supported by C-SPIN, one of the six SRC STARnet Centers, sponsored by MARCO and DARPA.

[1]H. Yu, R. Huber, T. Schwarze, F. Brandl, T. Rapp, P. Berberich, G. Duerr, and D. Grundler, Appl. Phys. Lett. **100**, 262412 (2012).
[2]A. Conca, J. Greser, T. Sebastian, S. Klingler, B. Obry, B. Leven, and B. Hillebrands, J. Appl. Phys. **113**, 213909 (2013).
[3]T. Schwarze and D. Grundler, Appl. Phys. Lett. **102**, 222412 (2013).
[4]A. A. Serga, A. V. Chumak, and B. Hillebrands, J. Phys. Appl. Phys. **43**, 264002 (2010).
[5]Y. Sun, H. Chang, M. Kabatek, Y.-Y. Song, Z. Wang, M. Jantz, W. Schneider, M. Wu, E. Montoya, B. Kardasz, B. Heinrich, S. G. E. te Velthuis, H. Schultheiss, and A. Hoffmann, Phys. Rev. Lett. **111**, 106601 (2013).
[6]H. Yu, O. d'Allivy Kelly, V. Cros, R. Bernard, P. Bortolotti, A. Anane, F. Brandl, R. Huber, I. Stasinopoulos, and D. Grundler, Sci. Rep. **4**, 6848 (2014).

[7]R. Hertel, W. Wulfhekel, and J. Kirschner, Phys. Rev. Lett. **93**, 257202 (2004).
[8]S.-K. Kim, J. Phys. Appl. Phys. **43**, 264004 (2010).
[9]S. Choi, K.-S. Lee, K. Y. Guslienko, and S.-K. Kim, Phys. Rev. Lett. **98**, 87205 (2007).
[10]A. Khitun, D. E. Nikonov, M. Bao, K. Galatsis, and K. L. Wang, Nanotechnology **18**, 465202 (2007).
[11]S.-K. Kim, K.-S. Lee, and D.-S. Han, Appl. Phys. Lett. **95**, 82507 (2009).
[12]S. Bance, T. Schrefl, G. Hrkac, A. Goncharov, D. A. Allwood, and J. Dean, J. Appl. Phys. **103**, 07E735 (2008).
[13]A. Khitun, M. Bao, and K. L. Wang, J. Phys. Appl. Phys. **43**, 264005 (2010).
[14]X. Wang, G. Guo, Y. Nie, G. Zhang, and Z. Li, Phys. Rev. B **86**, 54445 (2012).
[15]J.-S. Kim, M. Stärk, M. Kläui, J. Yoon, C.-Y. You, L. Lopez-Diaz, and E. Martinez, Phys. Rev. B **85**, 174428 (2012).
[16]X. S. Wang, P. Yan, Y. H. Shen, G. E. W. Bauer, and X. R. Wang, Phys. Rev. Lett. **109**, 167209 (2012).
[17]S. Woo, T. Delaney, and G. S. D. Beach, Nat. Phys. **13**, 448 (2017).
[18]S.-M. Seo, K.-J. Lee, H. Yang, and T. Ono, Phys. Rev. Lett. **102**, 147202 (2009).
[19]L. Liu, R. A. Buhrman, and D. C. Ralph, e-print arXiv:11113702 [Cond-Mat].
[20]L. Liu, O. J. Lee, T. J. Gudmundsen, D. C. Ralph, and R. A. Buhrman, Phys. Rev. Lett. **109**, 96602 (2012).
[21]S. Emori, U. Bauer, S.-M. Ahn, E. Martinez, and G. S. D. Beach, Nat. Mater. **12**, 611 (2013).
[22]L. Liu, C.-F. Pai, Y. Li, H. W. Tseng, D. C. Ralph, and R. A. Buhrman, Science **336**, 555 (2012).
[23]C.-F. Pai, L. Liu, Y. Li, H. W. Tseng, D. C. Ralph, and R. A. Buhrman, Appl. Phys. Lett. **101**, 122404 (2012).
[24]J. C. Slonczewski, J. Magn. Magn. Mater. **247**, 324 (2002).
[25]A. Brataas, A. D. Kent, and H. Ohno, Nat. Mater. **11**, 372 (2012).
[26]V. E. Demidov, S. Urazhdin, A. B. Rinkevich, G. Reiss, and S. O. Demokritov, Appl. Phys. Lett. **104**, 152402 (2014).
[27]K. An, D. R. Birt, C.-F. Pai, K. Olsson, D. C. Ralph, R. A. Buhrman, and X. Li, Phys. Rev. B **89**, 140405 (2014).
[28]M. Evelt, V. E. Demidov, V. Bessonov, S. O. Demokritov, J. L. Prieto, M. Muñoz, J. Ben Youssef, V. V. Naletov, G. de Loubens, O. Klein, M. Collet, K. Garcia-Hernandez, P. Bortolotti, V. Cros, and A. Anane, Appl. Phys. Lett. **108**, 172406 (2016).
[29]O. Gladii, M. Collet, K. Garcia-Hernandez, C. Cheng, S. Xavier, P. Bortolotti, V. Cros, Y. Henry, J.-V. Kim, A. Anane, and M. Bailleul, Appl. Phys. Lett. **108**, 202407 (2016).
[30]L. D. Landau and E. Lifshitz, Phys. Z. Sowjet **8**, 101–114 (1935).
[31]T. L. Gilbert, Phys. Rev. **100**, 1243 (1955).
[32]M. J. Donahue and D. G. Porter, OOMMF User's Guide, Version 1.0. Interagency Report No. NISTIR 6376, National Institute of Science and Technology, Gaithersburg, MD (1999), See http://math.nist.gov/oommf.
[33]J.-C. Rojas-Sánchez, N. Reyren, P. Laczkowski, W. Savero, J.-P. Attané, C. Deranlot, M. Jamet, J.-M. George, L. Vila, and H. Jaffrès, Phys. Rev. Lett. **112**, 106602 (2014).
[34]M. Weiler, J. M. Shaw, H. T. Nembach, and T. J. Silva, IEEE Magn. Lett. **5**, 1 (2014).
[35]Y. Tserkovnyak, A. Brataas, and G. E. W. Bauer, Phys. Rev. Lett. **88**, 117601 (2002).
[36]R. W. Damon and J. R. Eshbach, J. Phys. Chem. Solids **19**, 308 (1961).
[37]H. Benson and D. L. Mills, Phys. Rev. **178**, 839 (1969).
[38]R. P. Erickson and D. L. Mills, Phys. Rev. B **43**, 10715 (1991).
[39]J. Jorzick, S. O. Demokritov, B. Hillebrands, M. Bailleul, C. Fermon, K. Y. Guslienko, A. N. Slavin, D. V. Berkov, and N. L. Gorn, Phys. Rev. Lett. **88**, 47204 (2002).
[40]J. P. Park, P. Eames, D. M. Engebretson, J. Berezovsky, and P. A. Crowell, Phys. Rev. Lett. **89**, 277201 (2002).